Acta Pharmaceutica Sinica B 2021;11(11):3595−3607

Chinese Pharmaceutical Association
Institute of Materia Medica, Chinese Academy of Medical Sciences

Acta Pharmaceutica Sinica B

www.elsevier.com/locate/apsb
www.sciencedirect.com

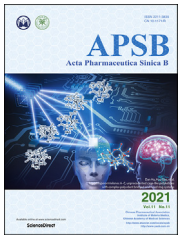

ORIGINAL ARTICLE

Self-assembled ternary hybrid nanodrugs for overcoming tumor resistance and metastasis

Xu Cheng[a,b,†], Dapeng Li[a,†], Jiaxi Xu[a], Bing Wei[c], Qin Fang[a], Longshun Yang[a], Yanbing Xue[a], Xin Wang[a], Rupei Tang[a,*]

[a]*Engineering Research Center for Biomedical Materials, Anhui Key Laboratory of Modern Biomanufacturing, School of Life Sciences, Anhui University, Hefei 230601, China*
[b]*School of Life Sciences, Anqing Normal University, Anqing 246133, China*
[c]*School of Biology and Food Engineering, Fuyang Normal University, Fuyang 236037, China*

Received 19 January 2021; received in revised form 21 March 2021; accepted 22 March 2021

KEY WORDS

Drugs dimer;
Multidrug resistance;
Metastasis;
Charge reversal;
Proton sponge;
Redox sensitive;
Polyethyleneimine;
Inflammation

Abstract Traditional chemotherapy exhibits a certain therapeutic effect toward malignant cancer, but easily induce tumor multidrug resistance (MDR), thereby resulting in the progress of tumor recurrence or metastasis. In this work, we deigned ternary hybrid nanodrugs (PEI/DOX@CXB-NPs) to simultaneously combat against tumor MDR and metastasis. *In vitro* results demonstrate this hybrid nanodrugs could efficiently increase cellular uptake at pH 6.8 by the charge reversal, break lysosomal sequestration by the proton sponge effect and trigger drugs release by intracellular GSH, eventually leading to higher drugs accumulation and cell-killing in drug-sensitive/resistant cells. *In vivo* evaluation revealed that this nanodrugs could significantly inhibit MDR tumor growth and simultaneously prevent A549 tumor liver/lung metastasis owing to the specifically drugs accumulation. Mechanism studies further verified that hybrid nanodrugs were capable of down-regulating the expression of MDR or metastasis-associated proteins, lead to the enhanced anti-MDR and anti-metastasis effect. As a result, the multiple combination strategy provided an option for effective cancer treatment, which could be potentially extended to other therapeutic agents or further use in clinical test.

*Corresponding author. Tel./fax: +86 51 5105740.
E-mail address: tangrp99@iccas.ac.cn (Rupei Tang).
[†]These authors made equal contributions to this work.
Peer review under responsibility of Chinese Pharmaceutical Association and Institute of Materia Medica, Chinese Academy of Medical Sciences.

https://doi.org/10.1016/j.apsb.2021.03.041

1. Introduction

Chemotherapy is one of the most common method for cancer therapy, which widely used in primary tumor or postoperative adjuvant treatment in clinical practice. However, when treatment with small molecule anticancer drugs for a long time, it much easily induces tumor multidrug resistance (MDR) or cells phenotypic change, which cause tumor recurrence or metastatic spreading to normal organs (such as liver and lung)[1−3]. This is one of the main reason for the inefficiency or failure of chemotherapy. Another one factor is the serious side effects of therapeutic drugs *in vivo*, such as the cardiotoxicity of doxorubicin and the nephrotoxicity of cisplatin[4,5]. Thus, there is urgent demand to develop advanced chemotherapeutic agents or formulations to block tumor MDR or metastasis, and as well as reducing systemic toxicity *in vivo*.

Recently, various nano-scale drugs delivery systems (nDDS) have been designed and developed by physical co-encapsulation or chemical bonding with different MDR/metastasis inhibitors (verapamil, resveratrol, quercetin, etc.) to ameliorate the above deficiencies[6−9]. Compared to traditional administration, these well-designed nDDS have many unique properties such as easily modification, targeting accumulation, controlled drugs release, etc[8,10]. In many cases, these nanosystems can block the function and expression of cytokines or proteins involved in tumor resistant/metastatic microenvironments, thereby leading to the desirable anti-MDR/metastasis effect[11,12]. However, there still remain some limitations hinder their clinical utilization, including the low loading efficiency, variation between batches, and carrier-related toxicity[13,14]. In response, novel nDDS based on carrier-free nanodrugs (pure drugs or drugs dimer) has attracted intensive interests[15−17]. The main advantages of this nanodrugs include simple fabrication process, higher drugs loading and precise drugs ratio, which is beneficial to scale-up production and clinical transformation[15,18]. For instance, Xiao et al.[19] constructed carrier-free nanocrystals from celastrol (CST) and doxorubicin (DOX), which efficiently induced apoptosis/autophagy by the down-regulation of P-glycoprotein (P-GP). Unfortunately, the debatable stability *in vivo* and no further modification of carrier-free nanodrugs limit their ability to cross tumor barriers including extracellular matrix, cytomembrane and acidic organelles[20,21]. Thus, it is very important to seek a balance between conventional nDDS and carrier-free nanodrugs for achieving more advanced treatment outcomes.

Herein, we developed the ternary hybrid nanodrugs by integrating the advantages of above nanosystems to improve *in vivo* drugs delivery, and as well as efficiently combat against tumor MDR/metastasis. This self-assembled nanosystem composed of two drugs dimer [doxorubicin (DOX) and celecoxib (CXB)] and a polyethylenimine (PEI) derivative (Fig. 1), denoted as PEI/DOX@CXB-NPs. On the one hand, DOX or CXB were linked *via* disulfide bonds and encapsulated inside particles through the $\pi-\pi$ stacking and hydrophobic interactions of the intermolecular aromatic planar rings[15,22], thus resulting in the superb drugs loading efficiency (DLE > 85%) (Supporting Information Table S1). Besides, DOX as a classic antitumor drug plays a major role in the process of cell death or apoptosis. And meanwhile, CXB as a nonsteroidal anti-inflammatory drug, is used to sensitize chemotherapy efficiency because of its ability to regulate inflammatory environments mediated MDR/metastasis protein in tumor regions[23−25]. Specially, compared to other synthetic or natural inhibitors, it can reduce the development cost, cycle time and risk owing to the availability of all relevant clinical data such as safety, dosing route or times[26,27]. On the other hand, PEI is a commercial cationic polymer, has been recognized as the efficient drugs/gene carriers because of its superior lysosomal escape ability by the proton sponge effect[28]. However, the high densities of cationic charge of PEI limits its circulation in the blood[28,29]. As such, herein, PEI was modified with DMMA and C18 for reconstructing its structure and function (Supporting Information Scheme S3), which could improve *in vivo* application.

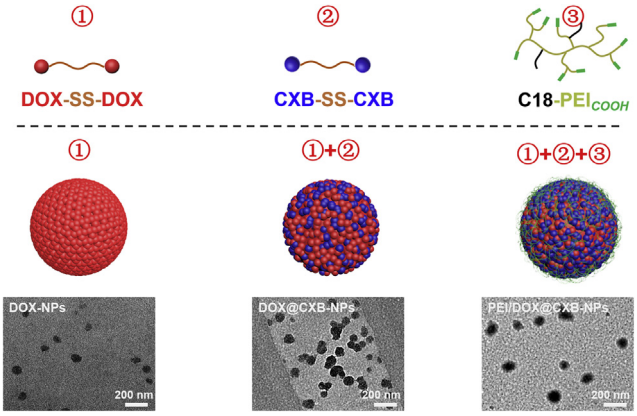

Figure 1 Self-assembly and TEM images of different nanodrugs particles.

Through the above ternary co-assembly, this combined nanosystem will achieve a stepwise targeting process from blood circulation to tumor cells: (i) reduce protein adsorption and remain stability for long-circulation in the blood vessels; (ii) passive accumulation at tumor tissue by the enhanced permeability and retention effect (EPR); (iii) charge reversal by the hydrolysis of β-carboxylic amides bonds under tumoral extracellular pH for enhanced cellular uptake[30,31]; (iv) trigger dual drugs release by the cleavage of disulfide in reductive milieu; (v) break lysosomal sequestration for high-efficiently exerting drugs activities; (vi) inhibit tumor cells resistance or metastasis by regulating protein levels. With the help of multiple synergistic effects, the hybrid nanosystem is capable to improve *in vivo* drugs delivery and significantly increase chemotherapeutic effects in breast or lung cancers.

2. Materials and methods

2.1. Materials

Polyethyleneimine (PEI, branched MW 10 KDa, 99%), celecoxib (CXB, 98%), stearic acid (C18) and *N*,*N*′-carbonyldiimidazole (CDI, 98%) were purchased from Energy Chemical Co., Ltd. (Shanghai, China). Doxorubicin hydrochloride (DOX·HCL) was purchased from Meilun Biological Technology (Dalian, China). Bis(2-hydroxyethyl) disulfide, 4-dimethylaminopyridine (DMAP), dimethylmaleic anhydride (DMMA), 1-(3-dimethylaminopropyl)-3-ethylcarbodiimide hydrochloride (EDC·HCL) and *N*-hydroxysuccinimide (NHS) were obtained from Mackin Biochemical Co., Ltd. (Shanghai, China). Cells apoptosis assay kit and cells cycle assay kit were purchased from Best Biotechnology Co., Ltd. (Shanghai, China). Primary antibody of P-gp was provide from Solarbio Science & Technology Co., Ltd. (Beijing, China). Human breast cancer cells (MCF-7 and MCF-7/ADR) and lung

cancer cells were obtained from KeyGen Biotech (Nanjing, China). Female BALB/c nude mice at the age of 5−6 weeks were purchased from the Cavens Laboratory Animal Limited Company (Changzhou, China). All other chemicals were analytical reagent and used without further purification.

2.2. Synthesis, preparation and characterization

Two drugs dimer linked by disulfide, and pH-sensitive PEI with grafting C18 and DMMA were synthesized, respectively. The detailed process was provided in Supporting Information. Single or hybrid nanodrugs particles were prepared by the nano-precipitation method[19]. The physical or chemical properties of above particles were carefully studied, as seen in Supporting Information.

2.3. Cellular uptake and subcellular co-localization

In order to cellular uptake behaviors, MCF-7 or MCF-7/ADR cells were seeded onto a confocal dish and cultured at 37 °C for 24 h. Then, cells were incubated with free DOX for 2 and 6 h. Afterward, cells were washed with PBS, fixed with 4% paraformaldehyde, stained with DAPI and observed by confocal laser scanning microscopy (CLSM, FluoView TM FV1000, Olympus, Japan). Besides, subcellular co-localization of nanodrugs particles was further carefully studied. In brief, cells were co-cultured with DOX-NPs and DOX@CXB-NPs at pH 7.4 medium, and/or co-cultured with PEI/DOX@CXB-NPs at pH 7.4 and 6.8 medium for 2 and 6 h. Then cells were incubated with 100 nmol/L Lyso-Tracker Green for 30 min. The next procedure was the same as above. Finally, cells were observed by CLSM at an excitation wavelength of 504 nm for lysosome and 594 nm for DOX.

2.4. In vitro P-gp expression

5×10^3 number of MCF-7/ADR cells were seeded in a 6-well plate and co-cultured with free DOX, DOX-NPs, DOX@CXB-NPs and PEI/DOX@CXB-NPs for 4 h. Then, the old medium was replaced with fresh culture medium and cultured for another 12 h. After that, cells were treated with lysis solution and collected, followed by immunoblotting analysis with P-gp antibody. The levels of P-GP protein were normalized against β-actin protein level.

2.5. In vitro cytotoxicity

The cell-killing effect of different formulations was evaluated by MTT assay. Briefly, cells (MCF-7, MCF-7/ADR and A549) were seeded into 96-well plates and cultured overnight. Then cells were cultured with free DOX, DOX-NPs, DOX@CXB-NPs, and PEI/DOX@CXB-NPs (pH 7.4 and 6.8) for 2 h, and RPMI1640 culture medium as the control. After that, the old medium was removed and new medium without drugs were added, and cultured for another 24 h. Finally, the supernatants were replaced with 200 μL culture medium containing MTT (5 mg/mL). After incubation for 4 h, the supernatants were removed and 150 μL DMSO solutions were added, and then shook for 10 min. Finally, the absorbance values of formazan in wells were measured at 570 nm by SpectraMax M2e Molecular devices. Cell viabilities were calculated by Eq. (1):

$$\text{Cell viabilities}\,(\%) = (A_{\text{sample}} - A_{\text{blank}})/(A_{\text{control}} - A_{\text{blank}}) \times 100 \quad (1)$$

2.6. In vitro wound healing, migration and invasion assay

To evaluate the wound healing, A549 cells were seeded on 12-well plates and cultured until the density of cells reached about 80%. Then, a 200 μL pipette tip was used to scratch a vertical wound, and each well was washed with PBS to remove floating cells. After that, cells were incubated with free CXB (1 μg/mL), free DOX, DOX-NPs, DOX@CXB-NPs and PEI/DOX@CXB-NPs for 24 and 48 h, and the equivalent DOX concentration was set at 1 μg/mL. The reparation of wounding area was observed and photographed at 0, 24 and 48 h by an inverted microscope. The wound healing rate was calculated using Eq. (2):

$$\text{Healing rate} = (A_t - A_0)/A_0 \quad (2)$$

where A represents the wound width.

Next, the migration and invasion assay were performed by the transwell device. A549 cells were incubated with the above samples for 24 h, then collected and re-suspended in serum-free culture medium. For the migration experiment, 5×10^4 number of treated cells (100 μL) were added in the upper chamber of transwells (insert 24-well plate, pore size of 8 μm), and 600 μL DMEM medium containing 10% FBS was added into the lower chambers. And cells treated with RPMI1640 medium were used as control. After culturing for 24 h, the upper cells were removed by a cotton swab, washed with PBS, fixed with 70% ethanol and stained with crystal violet. Finally, cells across the transwell chambers were photographed by an inverted fluorescence microscope, and the number of cells was counted. For the invasion experiment, 200 μL above cells (1×10^5) were added to the upper chambers coated with Matrigel (BD Bioscience, NY, USA). The next operations were the same as described in the migration assay.

2.7. Cells cycle and apoptosis

Cells cycle was assessed by flow cytometry (FCM, Becton Dickinson, USA). Briefly, MCF-7, MCF-7/ADR or A549 cells were co-cultured with free DOX, DOX-NPs, DOX@CXB-NPs and PEI/DOX@CXB-NPs (pH 7.4 and 6.8). After incubation for 24 h, cells were collected and fixed with 70% ethanol overnight at −20 °C. Then RNaseA (20 μg/mL) and PI (50 μg/mL) were added in cells suspensions and incubated for another 0.5 h in the dark. Finally, the distribution of cells cycle was detected by FCM.

Cells apoptosis was performed using an Annexin V-FITC/PI Dual Staining Kit. Briefly, cells were treated as mentioned above, then rinsed, separated and collected after digestion. Finally, cells were incubated with 5 μL Annexin V-fluorescein and propidium iodide (PI) in binding buffer, and then quantitatively detected by FCM.

2.8. In vivo drug metabolism and organs images

To evaluate the biological effect *in vivo*, the MDR tumor models were made *via* subcutaneous injection of MCF-7/ADR cells (1×10^6) diluted in matrigel into the back of BALB/c nude mice. When tumor volume reached 80−100 mm^3, *in vivo* experiments were carried out, and all operations were approved according to the protocols approved by Institutional Authority for Laboratory Animal Care of Anhui University, China.

To study *in vivo* drug metabolism, free DOX, DOX-NPs, DOX@CXB-NPs and PEI/DOX@CXB-NPs were intravenously injected into tumor-bearing mice at drug doses of 5 mg/kg, respectively ($n = 3$ for each group). At the predetermined time interval, blood was collected from the eyeball. Then mice were sacrificed and tumor mass were picked. After that, these samples were immersed in 4 mL of 70% ethanol containing 0.3 mol/L HCL, then homogenized, extracted for 48 h and centrifuged (3500 rpm) for 10 min (Micro17, Thermo Scientific Sorvall, USA). Finally, DOX concentration in supernatant was determined by a microplate reader at an excitation wavelength of 480 nm and emission wavelength of 590 nm. Besides, after injection for 24 h, mice were sacrificed and major organs were collected. These tissues were washed with ddH_2O and observed through the Maestro *In Vivo* Imaging System (Cambridge Research & Instrumentation Inc., USA).

2.9. *In vivo inhibition of tumor growth*

The above tumor-bearing mice were randomly divided into five groups ($n = 6$), then treated with free DOX, DOX-NPs, DOX@CXB-NPs and PEI/DOX@CXB-NPs (at equivalent dose of 5 mg/mL), by intravenous injection on Days 1, 7 and 14, and saline was used as the control. Then all tumor volumes and body weights were recorded every other day from Day 1. The tumor volume was calculated using Eq. (3):

$$V = (L \times S^2)/2 \quad (3)$$

where L and S represent the largest and shortest diameter, respectively.

At last, mice were sacrificed by cervical dislocation, and then tumor tissue were collected, photographed and weighted. Besides, after administration for 3 days, mice were sacrificed, and major organs including heart, liver, spleen, lung, kidney and tumor were collected. Then these tissues were sliced and stained with hematoxylin and eosin (H&E). Besides, tumor tissues were also stained with the TUNEL kit (Beijing solarbio science & technology Co., Ltd.). Finally, all tissues slices were observed and photographed by the inverted fluorescence microscope.

2.10. *In vivo inhibition of tumor metastasis*

In order to evaluate the anti-metastasis effect *in vivo*, mice were injected with A549 cells (2×10^6) through tail vein on the first day, and randomly separated into 5 groups (5 mice per group). After the lung metastasis model was established on Day 7, saline, free DOX, DOX-NPs, DOX@CXB-NPs and PEI/DOX@CXB-NPs were intravenously injected into mice, respectively. Mice were weighted every other day and sacrificed on Day 10. Then liver and lung tissues were collected and imaged, and the number of tumor nodules was counted. Besides, histological analysis of these organs was also observed by H&E staining.

2.11. *Immunohistochemical analysis*

A549 metastasis mice were treated with above samples for 3 days, then liver and lung tissues were collected, rinsed with ice PBS and immediately frozen at −80 °C. These tissues were cut to the thickness of 5 μm and incubated with fetal calf serum to block the non-specific binding. Then these samples were further stained with primary antibodies (MMP-9, E-cadherin, vimentin), goat anti-mouse IgG, S-A/HRP, 3,3-diaminobenzidin and hematoxylin (SP Kit, Solarbio). Finally, these slices samples were washed and observed by an optical microscope.

2.12. *Statistical analysis*

Significant differences were analyzed through Student's *t*-test. All quantitative results were obtained from at least triplicate samples. Data are presented as mean ± SD. $^*P < 0.05$ is considered statistically significant, and $^{***}P < 0.01$ and $^{***}P < 0.001$ are considered highly significant.

3. Results and discussion

3.1. *Synthesis and characterization*

The synthetic routes of DOX or CXB dimer (DOX−SS−DOX and CXB−SS−CXB), and pH-sensitive PEI (C18-PEI_{COOH}) were presented in Supporting Information Schemes S1−S3. The chemical properties of above products were verified *via* ^{1}H NMR, FI-TR and ESI-MS (Supporting Information Figs. S1–S7). Besides, the grafting ratio of C18 and DMMA in C18-PEI_{COOH} were 24.31% and 72.16%, respectively.

Single or hybrid nanodrugs particles were fabricated by the nanoprecipitation method and the assembly process was presented in Fig. 1. TEM images demonstrated that three nanoparticles had nearly spherical structure with the size of 100−150 nm. In addition, compared to carrier-free particles, ternary hybrid nanodrugs displayed a thin hydrophilic shell on its outside, which was derived from amphiphilic PEI. Besides, the hydrodynamic diameter of particles were further evaluated by DLS, results showed that the average size of particles were 118.9−142.5 nm with the PDI of 0.22−0.24 (Supporting Information Fig. S8A−S8C) in an aqueous solution. SEM images further confirmed the spherical shape of these particles, but their size was slightly lower than DLS results owing to the dehydration effect (Fig. S8D−S8F). In order to verify the particles composition, the energy dispersive spectrometry (EDS) were performed by SEM. Single DOX-NPs contained the elements of N, O and S, suggesting the existence of DOX and disulfide linker in particles (Fig. S8G). The elements of N, O, S and F existed in DOX@CXB-NPs, indicating the hybridization of DOX and CXB dimer (Fig. S8H). Besides, ternary hybrid particles had the same elements as binary hybrid particles, but the nitrogen content was significantly increased, which was ascribed to the wrapped PEI in particles (Fig. S8I). These results fully demonstrate that single or hybrid particles were successfully prepared, and the driving force of assembly mainly came from hydrogen bond effect, hydrophobic interaction and π–π stacking[15,22].

The surface properties of nanodrugs were further evaluated. Zeta potential exhibited that three particles had a negative charge because of the consuming of amino groups in drug molecules or polymers (Supporting Information Fig. S9A). Besides, we also found that PEI/DOX@CXB-NPs had lower potential (~30 mV) than that of other groups, which was attributed to the introduction of more carboxyl groups through the ring opening reaction with DMMA. As a result, the negative charge of particles might reduce the nonspecific adsorption and facilitate the delivery of nanosystems *in vivo*[32]. Fig. 2A confirmed this speculation, compared to cationic PEI, three nanodrugs both displayed stronger anti-absorption toward BSA, especially in PEI/DOX@CXB-NPs.

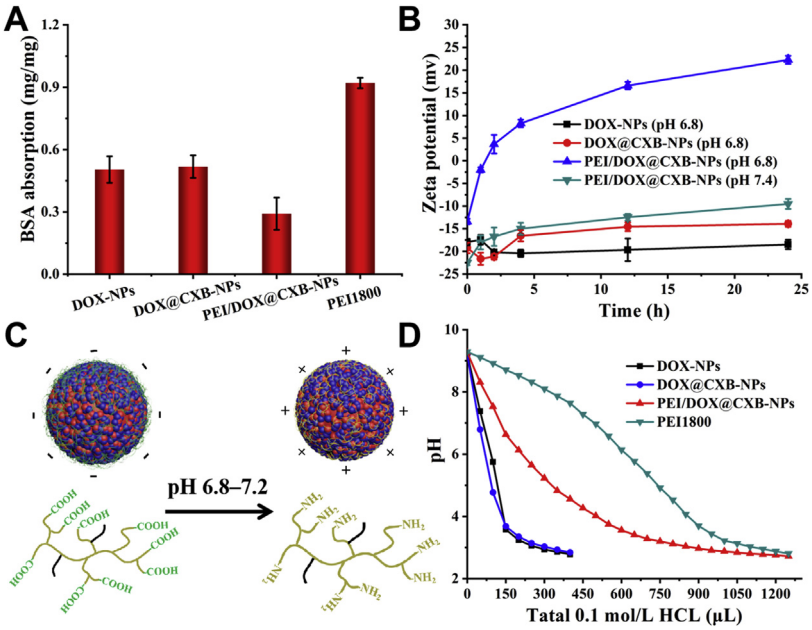

Figure 2 Anti-absorption of BSA protein (A); The change of surface charge at different pH (B); Data are presented as mean ± SD (n = 3). The diagram of charge reversal (C); Proton buffer evaluation (D).

Furthermore, the physiological stability of particles were monitored in the medium containing 10% FBS by DLS and results were presented in Fig. S9B and S9C. Notably, DOX-NPs and DOX@CXB-NPs had a certain rise on the size and PDI, while PEI/DOX@CXB-NPs just exhibited slightly fluctuations. This phenomenon demonstrated that self-assembled particles containing amphiphilic polymers might be more stable than hydrophobic nanodrugs, which was attributed to the protective effect of hydrophilic layers.

Previous studies have shown that β-carboxylic amides groups formed by the opening ring reaction with anhydrides remained stable in neutral environment while triggering the hydrolysis in mildly acidic condition[30]. This anhydrides included 2,3-dimethylmaleic anhydride (DMMA), cis-aconitic anhydride (CA), 1,2-dicarboxylic-cyclohexene anhydride (DCA) and hexahydro-3,6-epoxyphthalic anhydride (NCTD)[30,31,33,34]. Among them, the β-carboxylic amides from DMMA is more sensitive in response to low pH (6.8−7.2), which facilitates the design of nanosystems with charge reversal[31]. As shown in Fig. 2B, PEI/DOX@CXB-NPs displayed the rapid charge transitions in a short time at pH 6.8, and the potential reached to 8.26 mV at 4 h. However, the particles kept the negative charge at pH 7.4 within 24 h. The distinct charge reversal was attributed to the shedding of carboxyl groups from particles, leading to the exposure of more amino groups (Fig. 2C). In addition, DOX-NPs and DOX@CXB-NPs also displayed negative charge at low pH. In other word, the β-carboxylic amides in modified PEI played a major role on the charge transitions.

It is well known that cationic polymers have relatively strong buffer capacity, which facilitates the escape of nanosystems from the lysosome/endosome, that is ''proton sponge'' effect[35]. As shown in Fig. 2D, DOX-NPs and DOX@CXB-NPs had no obvious buffer ability, but PEI/DOX@CXB-NPs could neutralize more HCL, suggesting the protonation of secondary/tertiary amines groups. Besides, the buffer effect of PEI/DOX@CXB-NPs was lower than pure PEI because of the loss of $-NH_2$. As a result, the considerable buffering capacity of ternary nanodrugs might break drug sequestration in cytoplasmic vesicles[28,29], thereby high-efficiently exerting drugs activities.

3.2. *Reduction responsiveness and in vitro drug release*

Herein, disulfide bonds were used as a reduction-sensitive linker to take part in the assembly of particles. Thus, the reduction sensitivities of three particles were further evaluated. As shown in Fig. S9D−S9F, the diameter of particles continuously rose in the presence of 10 mmol/L DTT and accompanied by a non-uniform distribution. After treatment for 12 h, the mean size increased to 350−550 nm and the PDI were within 0.25−0.5. This result indicated the cleavage of disulfide linker (−SS−) under reductive substances (*e.g.*, DTT and GSH), and the formed sulfydryl (−SH) further underwent intramolecular nucleophilic substitution that released drugs (Fig. S10)[36,37]. Then the exposed amino groups of drugs amplified intermolecular repulsion of particles, leading to the increasing size of particles. In order to verify the above results, the morphology change of particles at 12 h was observed by TEM (Fig. S9G-S9I). Clearly, three particles showed a disorganized distribution with a large size, suggesting the dissociation process of particles. As a result, the destruction of the internal structure caused the instability of particles, which might accelerate drugs release.

Based on this, *in vitro* drugs release was performed in DTT solution. As shown in Fig. 3A–C, the release ratio of DOX (red curve) in three nanodrugs were significantly increased in the presence of 10 mmol/L DTT, and the cumulative release amount reached 53.72%−64.03% within 24 h. Besides, CXB exhibited a similar release patterns, and the cumulative release reached to 73.47% and 76.19% for DOX@CXB-NPs and PEI/DOX@CXB-NPs, respectively. Inversely, less than 10% DOX or CXB was released in no DTT solution for single or hybrid nanodrugs particles. As a result, these particles could well hold drugs in normal

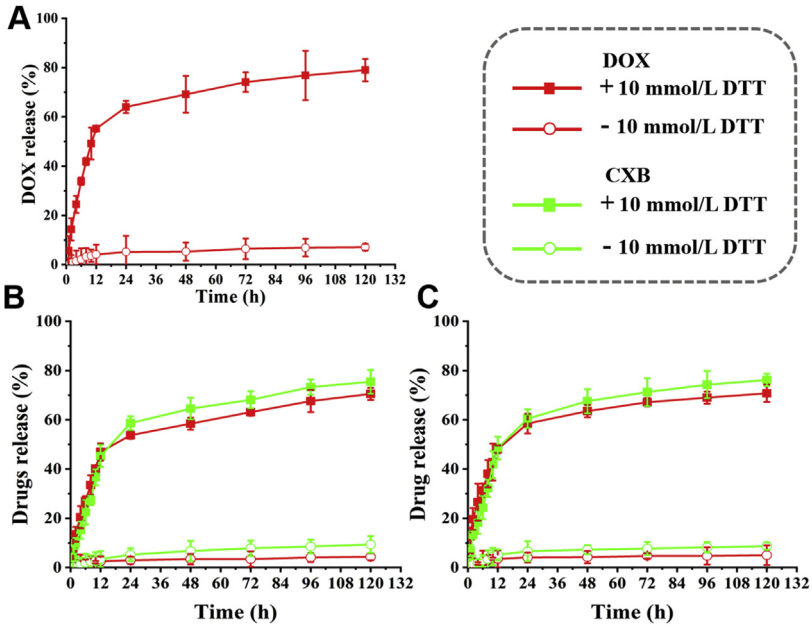

Figure 3 *In vitro* drugs release in PB solution with or without DTT for DOX-NPs (A), DOX@CXB-NPs (B) and PEI/DOX@CXB-NPs (C). Data are presented as mean ± SD ($n = 3$).

physiology condition while efficiently triggering drug release in reductive milieu of tumor.

3.3. *In vitro cellular uptake, subcellular co-localization and cytotoxicity*

In vitro cellular uptake of free DOX was evaluated using MCF-7 and MCF-7/ADR cells by CLSM. In MCF-7 cells, the red fluorescence was located in cytoplasm after incubation for 2 h (Fig. 4A$_1$), and accompanied by a dispersive distribution, suggesting the free diffusion into cells for small molecule drugs. With the time prolonging (6 h), the red signal was mainly observed in nucleus region, which was closely related to the DNA synthesis inhibition by DOX (Fig. 4A$_2$). The similar results were observed in MCF-7/ADR cell but with some difference. Whether in cytoplasm or nucleus, the DOX fluorescence intensity in MCF-7/ADR cells was much lower than that of MCF-7 cells, indicating a large number of drugs effluxes in MDR cells.

Then cell internalization and intracellular distribution behaviors of nanodrugs particles were carefully studied by subcellular co-localization. When MCF-7 cells were cultured in pH 7.4 medium for 2 h, three nanodrugs were mainly observed in acidic organelles (lysosomes/endosomes) and exhibited a dotted distribution owing to the endocytosis effect (Fig. 4B$_1$). However, when the pH of medium was adjusted to 6.8, PEI/DOX@CXB-NPs displayed stronger red signals in cytoplasmic space, indicating more cells internalization. This significant difference was closely related to the charge reversal of ternary hybrid particles (Fig. 2B and C). As well known, the phospholipid bilayer on cells membranes is electronegative, and PEI/DOX@CXB-NPs showed positive charge at acidic environment by charge reversal[31]. Thus, the opposite charges attract each other, resulting in the enhanced cellular uptake. After incubation for 6 h, DOX signals from DOX-NPs or DOX@CXB-NPs simultaneously appeared inside and outside the nucleus, suggesting the efficient drug release triggered by intracellular GSH (Fig. 4B$_2$). It was worth noting that DOX staining from PEI/DOX@CXB-NPs were mainly observed in nucleus rather than cytoplasm, and displayed the highest fluorescence intensity at pH 6.8. Notably, PEI was capable of breaking drug sequestration in cytoplasmic vesicles by the proton sponge effect, thereby quickly delivering drugs to nucleus[28,29]. The similar results were observed in MCF-7/ADR cells but with some difference. Whether co-culturing for 2 or 6 h, single particles exhibited the lowest DOX staining, but relatively bright red fluorescence appeared in binary or ternary hybrid particles groups, especially in PEI/DOX@CXB-NPs at low pH (Fig. 4C$_{1-2}$). Undoubtedly, MDR cells directly mediated the drugs efflux because of the over-expressed transporter proteins, such as P-gp. However, CXB in hybrid particles could suppress this efflux effect and increased intracellular drugs concentration. The reversal mechanism was further evaluated by Western blot. As shown in Supporting Information Fig. S11, the levels of P-gp remarkably reduced in two hybrid particles groups, which proved the regulating ability of CXB toward P-gp[38,39]. All together, these results revealed that ternary nanodrugs could trigger multistage synergistically effects, resulting in higher drugs concentration and activity in drug-sensitive/resistant tumor cells.

To evaluate antitumor efficiency of nanodrugs particles, MTT assay was used to detect cells viabilities on A549, MCF-7 and MCF-7/ADR cells. As shown in Supporting Information Fig. S12A−S12C, free DOX and nanodrugs particles both showed dose-dependent cytotoxicity in three tumor cells. After treatment for 24 h, cells viabilities were 36.23%, 38.16% and 32.24% for free DOX, DOX-NPs and DOX@CXB-NPs in A549 cells, respectively. Cell viabilities were 32.02%, 36.91% and 33.18% in MCF-7 cells. But in MCF-7/ADR cells, the cell-killing abilities of free DOX and DOX-NPs were greatly suppressed, and approximately 70% cells remained high activities at the maximum drugs concentration. Inspiringly, DOX@CXB-NPs remained considerable inhibition effect toward MDR cells, and final viability was 42.52%. This result was attributed to the anti-MDR effect of CXB as mentioned above, and more drugs accumulation

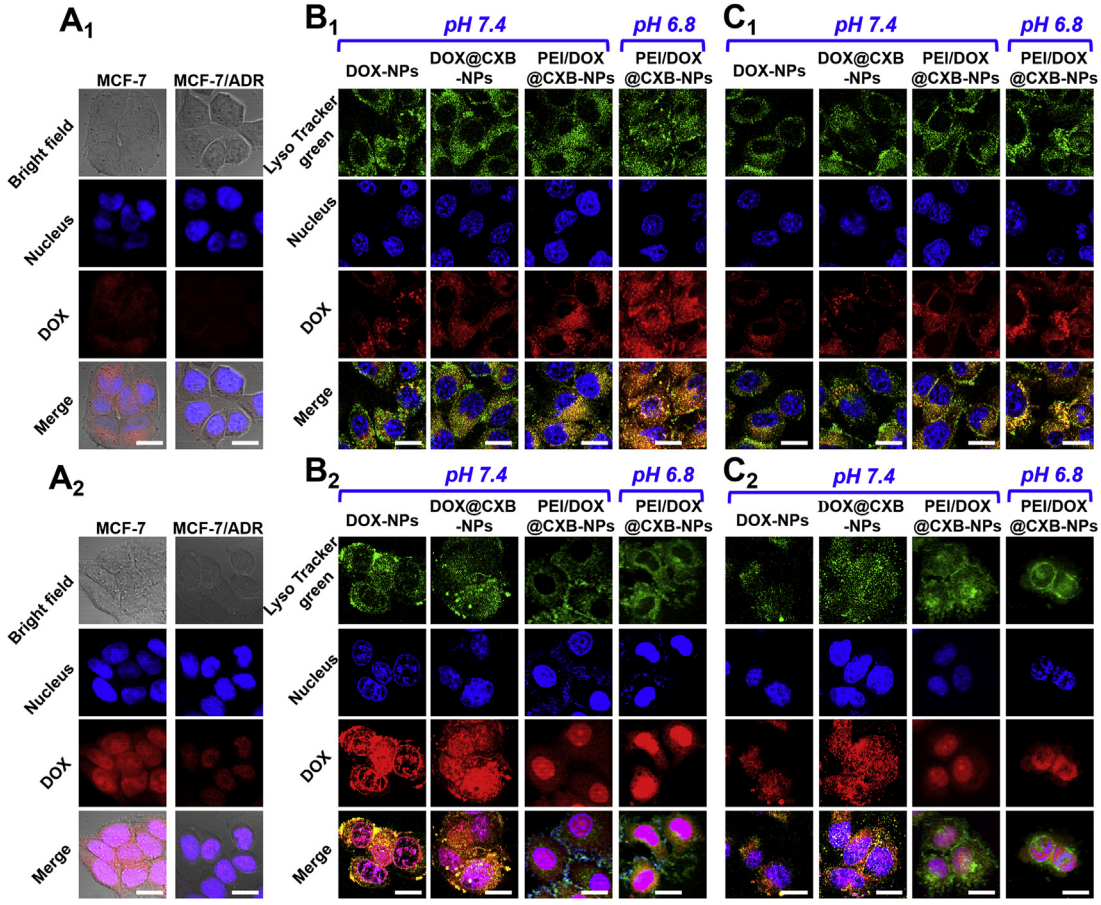

Figure 4 *In vitro* cellular uptake of free DOX at 2 h (A_1) and 6 h (A_2); Subcellular co-localization of nanodrugs particles in MCF-7 cells at 2 h (B_1) and 6 h (B_2); Subcellular co-localization of nanodrugs particles in MCF-7/ADR cells at 2 h (C_1) and 6 h (C_2); Scale bar = 15 μm.

led to higher cell-killing effect. It was noticeable that PEI/DOX@CXB-NPs showed stronger toxicity in three tumor cells compared to other DOX formulations at the same concentration (Fig. S12D–S12F). This effect was further amplified in pH 6.8 medium. The final viabilities were 28.5%, 23.48% and 32.85% for A549, MCF-7 and MCF-7/ADR cells, respectively. The greatly sensitized chemotherapy of ternary nanodrugs was probably attributed to more cellular uptake and faster escape from vesicles mediated by PEI derivatives. Finally, IC_{50} values were calculated and as shown in Fig. S12G–S12I. Single free DOX or DOX-NPs had relatively higher IC_{50}, especially in MDR cells (>150 μg/mL). While hybrid nanodrugs displayed lower IC_{50} in three tumor cells, the lowest IC_{50} appeared in PEI/DOX@CXB-NPs at pH 6.8. These results highlight the outstanding antitumor efficiency of ternary hybrid nanodrugs *in vitro*, which provided a strong support for tumor treatment *in vivo*.

3.4. *In vitro wound healing, migration and invasion evaluation*

The influence of nanodrugs on cells metastasis was carefully investigated. For the wound healing test, the scratch damage zone of control group was gradually filled by cells at 24 h and completely disappeared at 48 h, suggesting the strong motility of A549 cells (Fig. 5A). When incubated with different samples at low dosage, free DOX and DOX-NPs showed modest inhibition on scratch healing, while free CXB or hybrid nanodrugs could efficiently prevent cells migration. The healing rate were calculated in Fig. 5D, and results demonstrated that PEI/DOX@CXB-NPs possessed the highest anti-migration effect ($P < 0.001$), followed by DOX@CXB-NPs ($P < 0.01$). Furthermore, the Transwell migration test suggested DOX or CXB formulation could reduce the number of cell crossing through thin membrane to some extent (Fig. 5B). The migration inhibition rates (*vs.* control) were 53.31%, 39.93%, 35.1%, 61.16% and 69.96% for free DOX, free CXB, DOX-NPs, DOX@CXB-NPs and PEI/DOX@CXB-NPs, respectively (Fig. 5E). Notably, the hybrid nanodrugs presented the satisfactory outcomes on migration inhibition ($P < 0.001$ or $P < 0.01$). Besides, the similar invading restriction effect was observed in Transwell invasion test (Fig. 5C). DOX@CXB-NPs and PEI/DOX@CXB-NPs could reduce 62.27% and 73.31% of A549 cells invasion (Fig. 5F). Overall, these results indicate that CXB could efficiently restrict cells metastasis, and hybrid particles combined with DOX led to the best anti-metastasis effect.

3.5. *In vitro cell cycle and apoptosis*

The effects of various DOX formulations on cell cycle were further determined by FCM, and results were presented in Supporting Information Fig. S13. Compared to the control, free DOX or DOX-NPs induced obvious cell cycle arrest in G2/M phase in drugs-sensitive cells. The percentage of cells of G2/M

phase increased to 14.02%−14.27% and 10.97%−17.42% for A549 and MCF-7 cells, respectively (Fig. 6A and B). However, these samples had slight influence on cells cycle distribution in MCF-7/ADR cells owing to the very low intracellular drugs levels mediated by P-gp (Fig. 6C). When treatment with hybrid nanodrugs, the percentage of cells in G0/G1 phase remarkably increased, but cells accumulated in S and G2/M phase much decreased for three tumor cells. This results directly showed the regulation role of CXB toward cells cycle, which was attributed to its ability to interfere with the expression or activity of cyclins and cyclin dependent kinases (CDK)[40,41]. Besides, we also found PEI/DOX@CXB-NPs at pH 6.8 induced the highest cycle arrest owing to more cellular uptake, and the number of cells in G0/G1 phase was 80.93%, 86.15% and 85.67% for A549, MCF-7 cells and MCF-7/ADR cells. Predictably, the efficient cycle arrest would delay cells division, which might modify cell growth processes, and eventually leading to cell apoptosis.

In order to confirm the apoptosis effects induced by nanodrugs particles, the apoptosis assay were also performed by FCM. When A549 or MCF-7 cells were treated with various DOX formulations, the cell population significantly rose in the early and late apoptosis area (Supporting Information S14A and S14B). The quantitation of total apoptosis demonstrated that PEI/DOX@CXB-NPs had higher apoptotic rate in A549 and MCF-7 cells (Fig. 6D and E). But in MCF-7/ADR cells, free DOX or DOX-NPs only induced less cells apoptosis and the rates were less 30% (Figs. S14C and Fig. 6F), which was due to the existence of drug resistance. Hybrid nanodrugs were able to overcome tumor MDR, resulting in the increased apoptosis. The final apoptotic rates were 58.8% for DOX@CXB-NPs, 58.9% and 62.7% for PEI/DOX@CXB-NPs at pH 7.4 and 6.8, respectively. These findings were consistent with MTT results and cells cycle analysis, which highlighted the superiority of hybrid particles on tumor therapy.

3.6. *In vivo pharmacokinetic and organs images*

Considering the good performance of hybrid nanodrugs *in vitro*, we further conducted *in vivo* animal experiments using MCF-7/ADR tumor-bearing mice. First, the pharmacokinetics of free DOX and nanodrugs particles were evaluated *via* intravenous injection. As shown in Fig. 7A, the drug concentration in the blood of mice treated free DOX displayed fast decreasing within 2 h, and final drug content just was 0.12% ID/g, suggesting the very short half-life of small molecule drugs (0.53 h). However, three

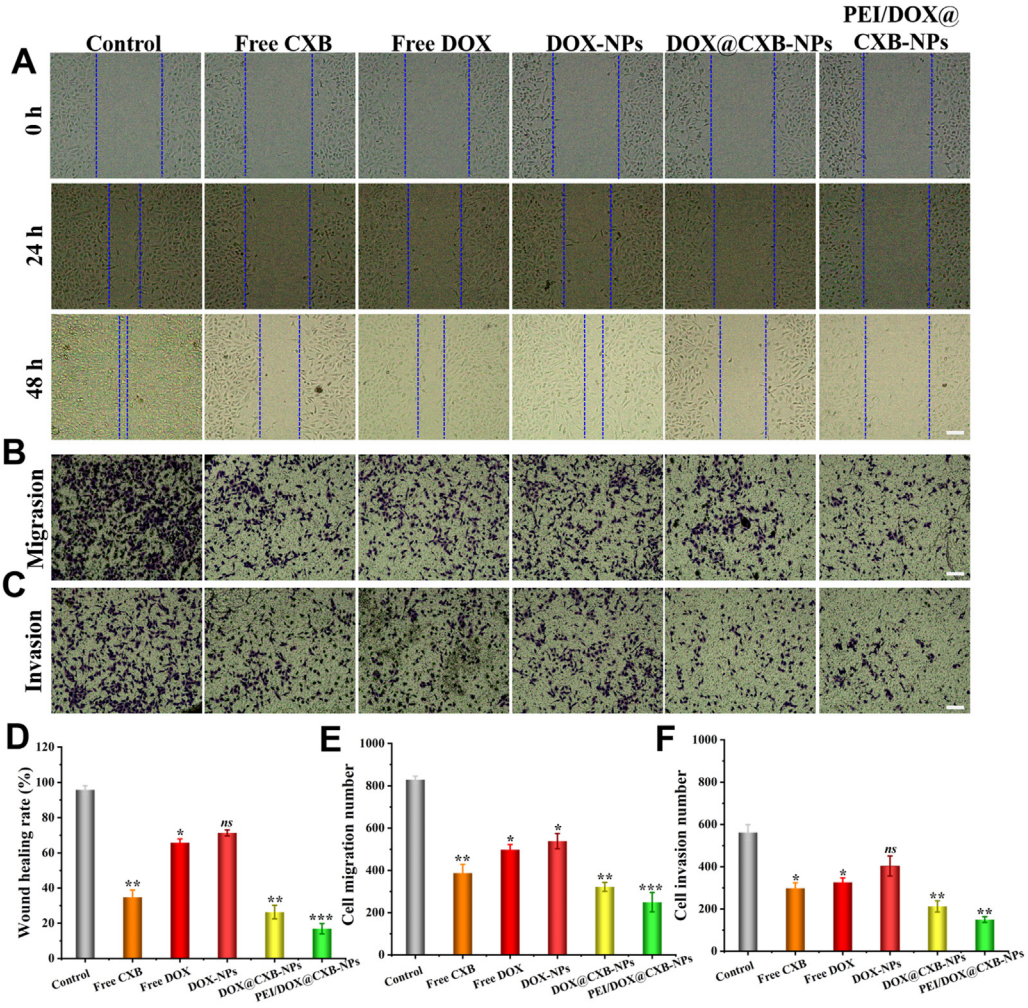

Figure 5 A549 cells wound healing (A) and healing rate (D); Cells migration evaluation (B) and migration number (E); Cells invasion evaluation (C) and invasion number (F); Scale bar = 20 μm. Data are presented as mean ± SD ($n = 6$); *$P < 0.05$, **$P < 0.01$, ***$P < 0.001$; *ns*, not significant.

nanodrugs had relatively gentle decreasing. Even at 24 h, 0.88%−1.47% ID/g DOX levels were detected. Obviously, the half-life of nanodrugs (8.15−10.16 h) were much higher than free DOX (Supporting Information Table S2). This significant difference indicated that nanodrugs could prolong the blood circulation owing to the relatively good stability or surface properties. Then, the accumulation of drugs in tumor site was further detected and results were presented in Fig. 7B. Three particles exhibited a gradually increased accumulation at tumor tissue and came to the peak at 12 h. Then the drug concentration slowly decreased, but still remained relatively high levels at 24 h (5.68%−8.51% ID/g). In contrast, free DOX in tumor site first showed accumulation after 1 h injection, following quickly decreased and final concentration only was 0.26% ID/g. An reasonable explanation was that the EPR effect at tumor site facilitated passive accumulation of particle with suitable size (10−200 nm), while limiting the retention of free drugs[42]. Meanwhile, the powerful MDR further accelerated the drugs clearance. *Ex vivo* tumor images at 24 h further confirmed the above results, and nanodrugs groups exhibited higher fluorescence signals than free DOX in tumor mass (Fig. 7C–D). Finally, we further evaluated DOX levels in tumor cells by slices analysis. As shown in Fig. 7E, PEI/DOX@CXB-NPs exhibited higher intracellular DOX staining than that of other particles, indicating more cellular internalization mediated by the charge attraction.

3.7. *In vivo antitumor and anti-metastasis evaluation*

To further assess the antitumor efficacy of nanodrugs *in vivo*, the above MDR tumor-bearing mice were injected with saline, free DOX, DOX-NPs, DXO@CXB-NPs and PEI/DOX@CXB-NPs, respectively. Several parameters including tumor volume, body weight and survival rate, were measured every other day. Fig. 8A shows the tumor volume change after injection three times. Clearly, free DOX or DOX-NPs slightly suppressed tumor growth compared to saline group, and final tumor volume were both over 500 mm^3, suggesting the weak therapeutic effect of them. The main reason was attributed to low drugs concentration in tumor site as mentioned above. However, hybrid nanodrugs displayed significant inhibition effect on tumor growth, and the tumor volumes (*vs.* saline) reduced 78.27% and 89.79% for DOX@CXB-NPs and PEI/DOX@CXB-NPs, respectively. Fig. 8B shows the tumor images at last day, and tumor masses with smaller size were found in two hybrid nanodrugs groups. Besides, the mean tumor weights were calculated in Fig. 8C, there was a significant difference on tumor weight between hybrid particles and other groups, indicating the excellent anticancer effect of them, especially in PEI/DOX@CXB-NPs ($P < 0.001$ or $P < 0.01$). Based on this, the tumor growth inhibition (TGI) against saline were 18.03%, 37.42%, 72.35% and 84.87% for free DOX, DOX-NPs, DOX@CXB-NPs and PEI/DOX@CXB-NPs, respectively (Fig. 8D). Pathological analysis was carried out to verify this results. TUNEL staining showed that little green fluorescence appeared in free DOX and DOX-NPs groups, while more green signals were observed in DOX@CXB-NPs and PEI/DOX@CXB-NPs groups (Fig. 8E). H&E staining further demonstrated the above particles caused higher tumor cells loss than single DOX groups, and accompanied by cell fragmentation and shrinkage (Fig. 8F). As a result, hybrid nanodrugs could significantly improve antitumor effects against MDR tumor, and the highest inhibitory growth appeared PEI/DOX@CXB-NPs, which was attributed to the multistage combination effects (Scheme 1), including: i) the good stability and surface property led to higher drug accumulations in tumor sites; ii) charge reversal mediated more cellular uptake; iii) the proton sponge effect broke drugs sequestration; (iv) high GSH concentration accelerated drugs release; (v) CXB down-regulated P-gp expression that reversed tumor MDR.

To evaluate the anti-metastasis effect of nanodrugs particles, A549 tumor metastasis models were established and used. After injection twice during 10 days, liver and lung tissue were picked, washed and photographed. As shown in Fig. 9A and B, the saline group showed serried tumor nodules in liver and lung tissues, suggesting the strong metastasis ability of A549 tumor cells.

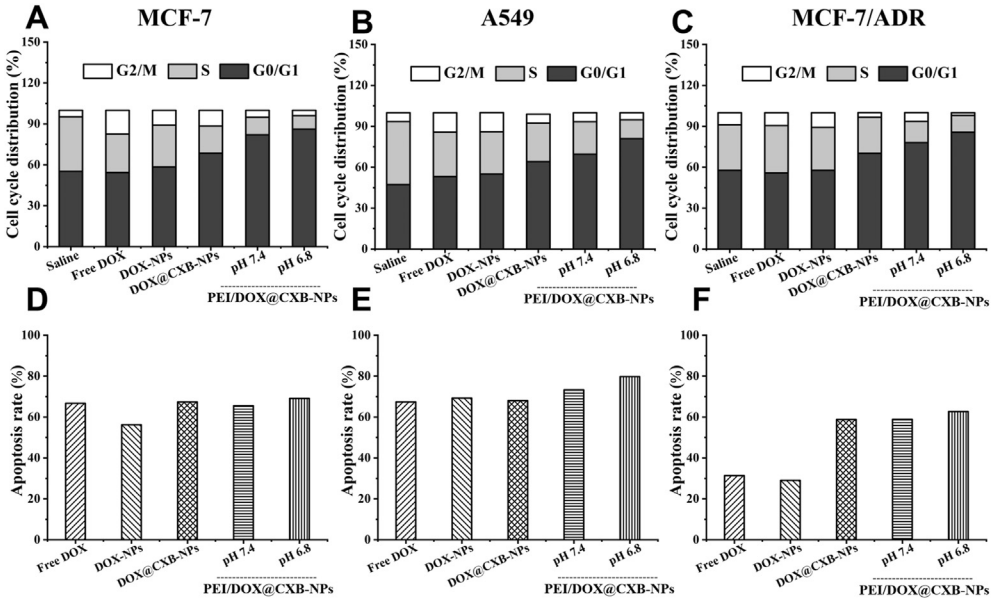

Figure 6 Cells cycle distribution in MCF-7 (A), MCF-7/ADR (B) and A549 (C) cells; Total apoptosis rate in MCF-7 (D), MCF-7/ADR (E) and A549 (F) cells.

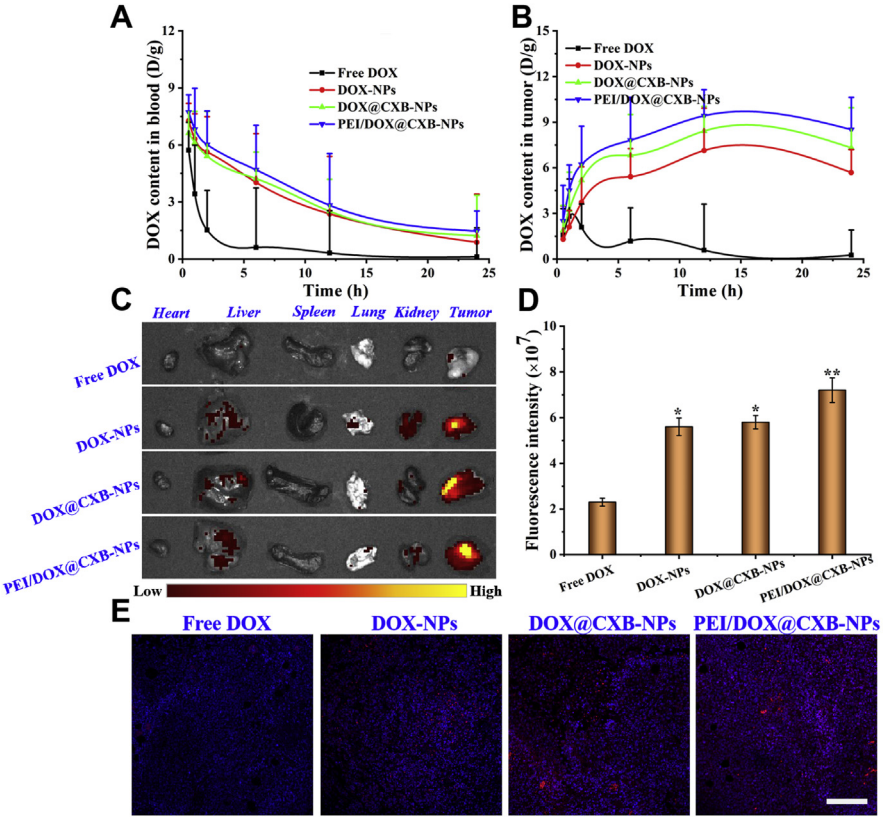

Figure 7 (A) Drug metabolism in blood ($n = 3$); (B) Drug accumulation in tumor ($n = 3$); (C) *Ex vivo* DOX fluorescence images and (D) Semi-quantitatively analysis of average fluorescence intensities ($n = 3$); DOX staining by H&E analysis (E), scale bar = 100 μm.

When treatment with various DOX formulations, the lesions of metastasis both decreased to some extent. Among them, free DOX showed slightly therapeutic effect on A549 liver/lung metastasis (Fig. 9C and D), but hybrid nanodrugs were more efficient in reducing metastatic nodules, especially in PEI/DOX@CXB-NPs group ($P < 0.001$). This result was further verified by H&E staining in Fig. 9E. Two hybrid particles exhibited a very small area of liver or lung micrometastatic lesion and accompanied by the decrease of tumor cells. Conversely, the distinct and extensive A549 metastasis colonies

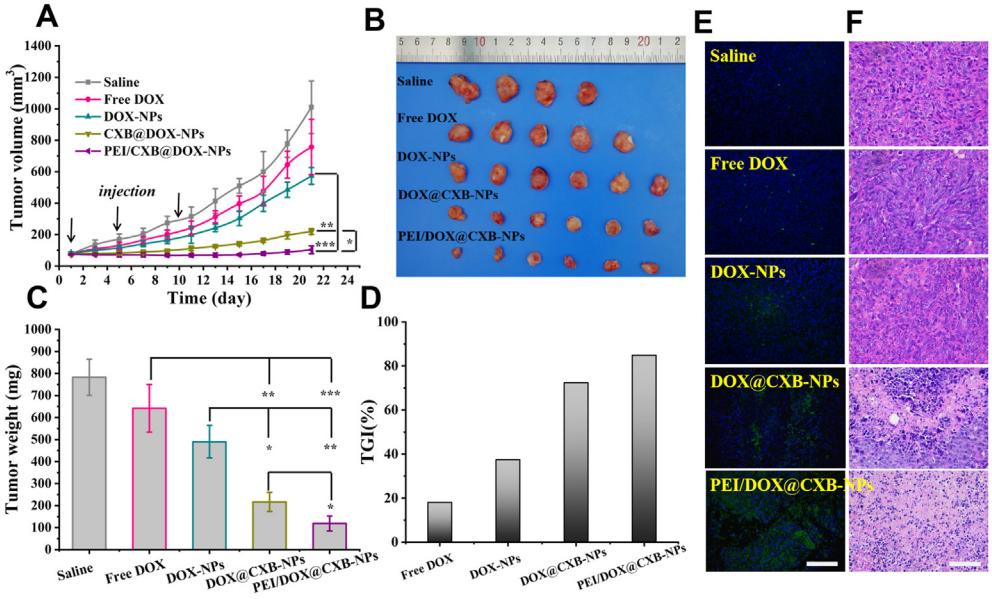

Figure 8 *In vivo* antitumor assessment: (A) Tumor volume change, data are presented as mean ± SD ($n = 6$); (B) Tumor tissue images; (C) Average tumor weight, data are presented as mean ± SD ($n = 5$); (D) Tumor growth inhibition; (E) TUNEL apoptosis and (F) H&E staining analysis of tumor tissue; Scale bar = 100 μm. $^*P < 0.05$, $^{**}P < 0.01$, $^{***}P < 0.001$.

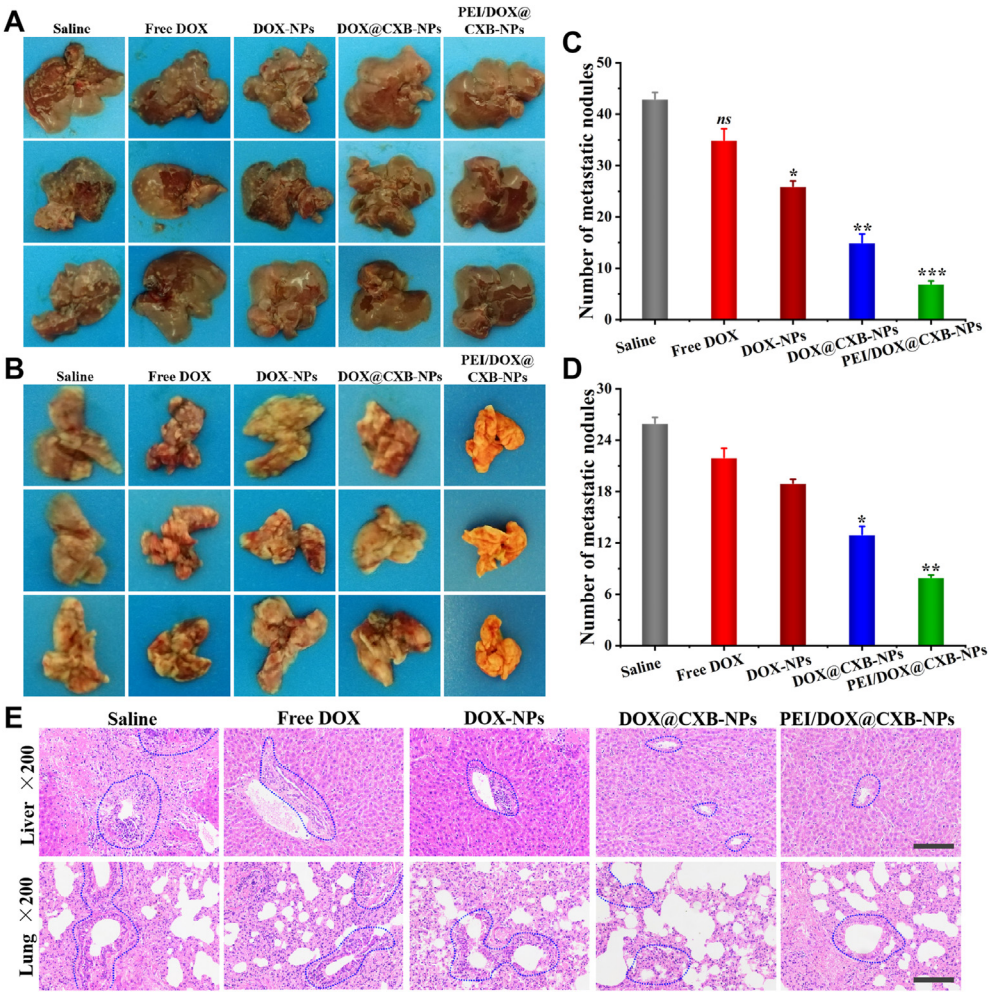

Figure 9 Representative images of liver (A) and lung (B) tissues from A549 tumor-bearing mice; Tumor nodule number in liver (C) and lung (D); Data are presented as mean ± SD ($n = 5$); H&E section analysis of liver and lung tissue, scale bar = 100 μm. *$P < 0.05$, **$P < 0.01$, ***$P < 0.001$.

were observed in free DOX, DOX-NPs and saline groups. These results were consistent with the anti-metastasis test *in vitro*, which fully revealed hybrid nanodrugs could efficiently suppress tumor progress and metastasis *in vivo*.

3.8. *Immunohistochemical analysis*

The anti-MDR and anti-metastasis mechanisms of nanodrugs particles *in vivo* were further studied by immunohistochemistry staining. As well known, the most common cause of tumor MDR is over-expressed efflux pumps such as P-gp. Thus, the levels of P-gp *in vivo* were firstly evaluated and as shown in Supporting Information Fig. S15. As similar to saline group, a mass of P-gp proteins (brown) were observed in single DOX formulations. However, hybrid nanodrugs groups exhibited a remarkably reduction on the expression of P-gp. This result implied that CXB could suppress the expression of P-gp, which was similar to previous reports[25]. In addition, free CXB also showed slightly inhibition effect on the generation of P-gp because of the low drugs accumulation in tumor sites.

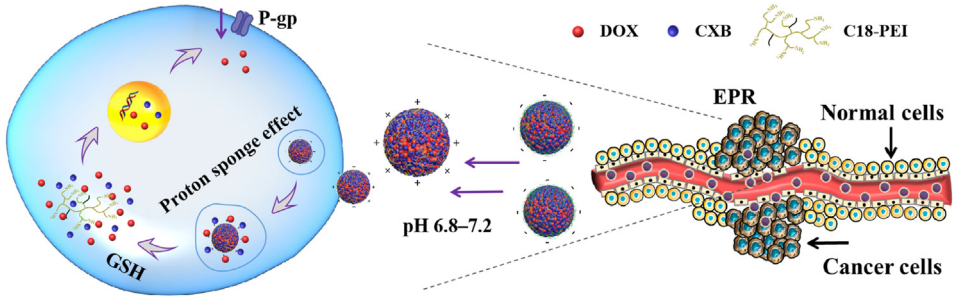

Scheme 1 *In vivo* delivery and works mechanism of PEI/DOX@CXB-NPs.

Tumor metastasis is complicated process involving extracellular matrix (ECM) degradation, angiogenesis, cell proliferation and phenotypic differentiation, etc[43,44]. For instance, matrix metalloproteinases (MMP-2 and MMP-9) can degrade the network of ECM, which allow tumor metastasis[43]. As shown in Supporting Information Fig. S16A and S16B, the specific MMP-9 proteins located in liver and lung were observed in DOX-NPs-treated group, but hardly no expression in DOX@CXB-NPs and PEI/DOX@CXB-NPs, which meant CXB in hybrid particles could inhibit the action of MMP-9. Besides, the up-regulated E-cadherin (marker of epithelial differentiation) and down-regulated vimentin (marker of mesenchymal state) were also observed in two hybrid particles compared with single particle, suggesting high cells differentiation[45,46]. In other word, the migratory and invasive abilities of tumor cells were greatly limited after co-treatment with DOX and CXB.

3.9. *In vivo* biosafety

In vivo biosafety of nanodrugs were carefully evaluated in MCF-7/ADR and A549 tumor bearing mice. First, the body weight of mice was monitored in Supporting Information Fig. S17A and S17B. Clearly, the saline group possessed a relatively high mice weight of 22−24 g, which was connected with the quickly proliferation and growth of tumors or metastasis colonies. On the contrary, an obvious decreasing of body weight was found in free DOX groups, suggesting the severe systemic toxicity. Besides, the mice treated with three nanodrugs exhibited a slight fluctuation on body weight. Clinical studies indicated the major limitation of DOX was serious cardiotoxicity *in vivo* owing to the nonspecific distribution. Therefore, these nanodrugs could improve the biocompatibility of drugs by increasing the stability in blood and specifically accumulating at tumor site. Further verification was performed by H&E staining and as shown in Supporting Information Fig. S18A and S18B, free DOX induced serious heart damage such as typical necrosis of muscle fibers, while no obvious morphological changes or tissue loss were observed in major organs of mice treated with nanodrugs particles. As a result, the quickly progressive tumors or severe systemic toxicity caused the death of mice during long-term treatment (Fig. S17C and S17D), while nanodrugs could significantly improve the survival rate of mice.

4. Conclusions

In this paper, we fabricated a ternary hybrid nanodrugs, which contained GSH-responsive DOX and CXB dimer inside particles, and its surface coating with pH-sensitive PEI copolymer. *In vitro* studies showed this nanosystem had acceptable physical and chemical properties, including small size, spherical shape, negative surface charge, low protein adsorption, high stability and GSH-triggered drug release. *In vitro* cells tests proved that hybrid PEI/DOX@CXB-NPs significantly increased cellular uptake at pH 6.8 medium by charge reversal and quickly escaped from acidic vesicles by the proton sponge effect. Then the released CXB efficiently inhibited drugs efflux by reducing the expression of P-gp, resulting in higher DOX concentration and toxicity in MCF-7/ADR cells. *In vivo* studies indicated hybrid nanodrugs had long-term blood-circulation and specific accumulation at tumor regions, which achieved better inhibition effect against MDR tumor as well as reducing side effect. Furthermore, this hybrid particles exhibited distinct therapeutic effect against A549 tumor liver/lung metastasis through regulating the expression of ECM-associated proteins. Overall, the multistage combination of ternary hybrid nanodrugs led to the superior anti-MDR and anti-metastasis effect *in vivo*, which can be further optimized for clinical treatment.

Acknowledgments

This work was supported by the National Natural Science Foundation of China (Nos. 51803001 and 51603001), the Research Foundation of Education Department of Anhui Province of China (Nos. KJ2018ZD003, KJ2018A0006 and KJ2019A0015), and the Academic and Technology Introduction Project of Anhui University (AU02303203, China).

Author contributions

Xu Cheng, Xin Wang and Rupei Tang designed the research. Xu cheng, Jiaxi Xu and Qin Fang carried out the experiments and performed data analysis. Being Wei, Longshun Yang and Yanbing Xue participated part of the experiments. Dapeng Li provided experimental drugs and quality control. Xu Cheng wrote the manuscript. Rupei Tang revised the manuscript. All of the authors have read and approved the final manuscript.

Conflicts of interest

The authors have no conflicts of interest to declare.

Appendix A. Supporting Information

Supporting data to this article can be found online at https://doi.org/10.1016/j.apsb.2021.03.041.

References

1. Assaraf YG, Brozovic A, Gonçalves AC, Jurkovicova D, Linē A, Machuqueiro M, et al. The multi-factorial nature of clinical multidrug resistance in cancer. *Drug Resist Update* 2019;**46**:100645.
2. Fernandes C, Prabhu P, Juvale K, Suares D, Yc M. Cancer cell fusion: a potential target to tackle drug-resistant and metastatic cancer cells. *Drug Discov Today* 2019;**24**:1836−44.
3. Zhong G, Liu S, Zheng Y, Lou W, Teo JY, Bao C, et al. Polymers with distinctive anticancer mechanism that kills MDR cancer cells and inhibits tumor metastasis. *Biomaterials* 2019;**199**:76−87.
4. Koleini N, Nickel BE, Edel AL, Fandrich RR, Ravandi A, Kardami E. Oxidized phospholipids in doxorubicin-induced cardiotoxicity. *Chem Biol Interact* 2019;**303**:35−9.
5. Babak MA, Zhi Y, Czarny B, Toh TB, Hooi L, Chow EK, et al. Dual-targeting dual-action platinum(IV) platform for enhanced anticancer activity and reduced nephrotoxicity. *Angew Chem Int Ed Engl* 2019;**131**:8193−206.
6. Leopoldo M, Nardulli P, Contino M, Leonetti F, Luurtsema G, Colabufo NA. An updated patent review on p-glycoprotein inhibitors (2011–2018). *Expert Opin Ther Pat* 2019;**29**:455−61.
7. Kumar A, Jaitak V. Natural products as multidrug resistance modulators in cancer. *Eur J Med Chem* 2019;**176**:268−74.
8. Yin Q, Shen J, Zhang ZW, Yu HJ, Li YP. Reversal of multidrug resistance by stimuli-responsive drug delivery systems for therapy of tumor. *Adv Drug Deliv Rev* 2013;**65**:1699−715.
9. Li R, Xie Y. Nanodrug delivery systems for targeting the endogenous tumor microenvironment and simultaneously overcoming multidrug resistance properties. *J Control Release* 2017;**251**:49−67.

10. Ahmad J, Akhter S, Ahmed Khan M, et al. Engineered nanoparticles against MDR in cancer: the state of the art and its prospective. *Curr Pharm Design* 2016;**22**:4360−73.
11. Yoon YJ, Han YM, Choi J, Lee YJ, Yun J, Lee SK, et al. Benproperine, an ARPC2 inhibitor, suppresses cancer cell migration and tumor Metastasis. *Biochem Pharmacol* 2019;**163**:46−54.
12. Rejinold NS, Yoo J, Jon S, Kim YC. Curcumin as a novel nanocarrier system for doxorubicin delivery to MDR cancer cells: *in vitro* and *in vivo* evaluation. *ACS Appl Mater Interfaces* 2018;**34**:28458−513.
13. Kamaly N, He JC, Ausiello DA, Farokhzad OC. Nanomedicines for renal disease: current status and future applications. *Nat Rev Nephrol* 2016;**12**:738−53.
14. Gao CX, Wei DL, Yang HL, Chen T, Yang L. Nanotechnology for treating osteoporotic vertebral fractures. *Int J Nanomed* 2015;**10**:5139.
15. Zhuang WR, Wang Y, Cui PF, Xing L, Lee J, Kim D, et al. Applications of π−π stacking interactions in the design of drug-delivery systems. *J Control Release* 2019;**294**:311−6.
16. Gao C, Bhattarai P, Chen M, Zhang N, Hameed S, Yue X, et al. Amphiphilic drug conjugates as nanomedicines for combined cancer therapy. *Bioconjugate Chem* 2018;**29**:3967−4015.
17. Yang XT, Hu C, Tong F, Liu H, Zhou Y, Qin L, et al. Tumor microenvironment-responsive dual drug dimer-loaded PEGylated bilirubin nanoparticles for improved drug delivery and enhanced immunechemotherapy of breast cancer. *Adv Funct Mater* 2019;**29**:1901896.
18. Li C, Lin JF, Wu PY, Zhao RR, Zou JJ, Zhou M, et al. Small molecule nanodrug assembled of dual-anticancer drug conjugate for synergetic cancer metastasis therapy. *Bioconjugate Chem* 2018;**29**:3495−502.
19. Xiao Y, Liu J, Guo M, Zhou H, Jin J, Liu J, et al. Synergistic combination cemotherapy of carrier-free celastrol and doxorubicin nanocrystals for overcoming drug resistance. *Nanoscale* 2018;**10**:12639−711.
20. Karaosmanoglu S, Zhou MJ, Shi BY, Zhang XJ, Williams GR, Chen XF. Carrier-free nanodrugs for safe and effective cancer treatment. *J Control Release* 2021;**329**:805−32.
21. Huang L, Zhao SJ, Fang F, Xu T, Lan MH, Zhang JF, et al. Advances and perspectives in carrier-free nanodrugs for cancer chemomonotherapy and combination therapy. *Biomaterials* 2011;**268**:120557.
22. Lin CC, Tong F, Liu R, Xie R, Lei T, Chen YX, et al. GSH-responsive SN38 dimer-loaded shape-transformable nanoparticles with iRGD for enhancing chemo-photodynamic therapy. *Acta Pharm Sin B* 2020;**10**:2348−61.
23. Xu C, Yang S, Jiang Z, Zhou J, Yao J. Self-propelled gemini-like LMWH-scaffold nanodrugs for overall tumor microenvironment manipulation *via* macrophage reprogramming and vessel normalization. *Nano Lett* 2020;**20**:372−83.
24. Shi LL, Xu L, Wu CW, Xue B, Jin X, Yang JP, et al. Celecoxib-induced self-assembly of smart albumin−doxorubicin conjugate for enhanced cancer therapy. *ACS Appl Mater Interfaces* 2018;**10**:8555−65.
25. Liu J, Chang B, Li Q, Xu L, Liu X, Wang G, et al. Redox-responsive dual drug delivery nanosystem suppresses cancer repopulation by abrogating doxorubicin-promoted cancer stemness, metastasis, and drug resistance. *Adv Sci* 2019;**6**:1801987.
26. Ashburn TT, Thor KB. Drug repositioning: identifying and developing new uses for existing drug. *Nat Rev Drug Discov* 2004;**3**:673−83.
27. Pushpakom S, Iorio F, Eyers PA, Escott KJ, Hopper S, Wells A, et al. Drug repurposing: progress, challenges and recommendations. *Nat Rev Drug Discov* 2019;**18**:41−58.
28. Cao Y, Huang HY, Chen LQ, Du HH, Cui JH, Zhang LW, et al. Enhanced lysosomal escape of pH-responsive polyethylenimine−betaine functionalized carbon nanotube for the codelivery of survivin small interfering RNA and doxorubicin. *ACS Appl Mater Interfaces* 2019;**11**:9763−76.
29. Gaspar VM, Baril P, Costa EC, Melo-Diogo DD, Foucher F, Queiroz JA, et al. Bioreducible poly(2-ethyl-2-oxazoline)-PLA-PEI-SS triblock copolymer micelles for co-delivery of DNA minicircles and doxorubicin. *J Control Release* 2015;**213**:175−91.
30. Li Y, Yang HY, Thambi T, Park JH, Lee DS. Charge-convertible polymers for improved tumor targeting and enhanced therapy. *Biomaterials* 2019;**217**:119299.
31. Zhou ZX, Shen YQ, Tang JB, Fan MH, Kirk EAV, Murdoch WJ, et al. Charge-reversal drug conjugate for targeted cancer cell nuclear drug delivery. *Adv Funct Mater* 2009;**19**:3580−9.
32. Elsabahy M, Wooley KL. Design of polymeric nanoparticles for biomedical delivery applications. *Chem Soc Rev* 2012;**41**:2545−61.
33. Xie S, Zhao L, Song X, Tang M, Mo C, Li X. Doxorubicin-conjugated *Escherichia coli* nissle 1917 swimmers to achieve tumor targeting and responsive drug release. *J Control Release* 2017;**268**:390−440.
34. H KD, Cao MZ, Mao WW, Sun XR, Tang JB, Shen YQ, et al. Targeted acid-labile conjugates of norcantharidin for cancer chemotherapy. *J Mater Chem* 2012;**22**:15804−11.
35. Zhang L, Yu M, Wang J, Tang R, Yan G, Yao W, et al. Low molecular weight PEI-based vectors *via* acid-labile ortho ester linkage for improved gene delivery. *Macromol Biosci* 2016;**16**:1175−87.
36. Xu J, Wang J, Luft JC, Tian S, Owens G, Pandya AA, et al. Rendering protein-based particles transiently insoluble for therapeutic applications. *J Am Chem Soc* 2012;**134**:8774−7.
37. Hu X, Hu J, Tian J, Ge Z, Zhang G, Luo K, et al. Polyprodrug amphiphiles: hierarchical assemblies for shape regulated cellular internalization, trafficking, and drug delivery. *J Am Chem Soc* 2013;**135**:17617−29.
38. Xu HB, Shen FM, Lv QZ. Celecoxib enhanced the cytotoxic effect of cisplatin in drug-resistant human gastric cancer cells by inhibition of cyclooxygenase-2. *Eur J Pharmacol* 2015;**769**:1−7.
39. Fantappiè O, Solazzo M, Lasagna N, Platini F, Tessitore L, Mazzanti R. P-glycoprotein mediates celecoxib-induced apoptosis in multiple drug-resistant cell lines. *Cancer Res* 2007;**67**:4915−23.
40. Kang KB, Zhu C, Yong SK, Gao Q, Wong MC. Enhanced sensitivity of celecoxib in human glioblastoma cells: induction of DNA damage leading to p53-dependent G 1 cell cycle arrest and autophagy. *Mol Cancer* 2009;**8**:66.
41. Tai Y, Zhang LH, Gao JH, Zhao C, Tong H, Ye C, et al. Suppressing growth and invasion of human hepatocellular carcinoma cells by celecoxib through inhibition of cyclooxygenase-2. *Cancer Manag Res* 2019;**11**:2831.
42. Huo D, Jiang XQ, Hu Y. Recent advances in nanostrategies capable of overcoming biological barriers for tumor management. *Adv Mater* 2019:1904337.
43. Balakrishnan S, Bhat FA, Raja Singh P, Mukherjee S, Elumalai P, Das S, et al. Gold nanoparticle-conjugated quercetin inhibits epithelial−mesenchymal transition, angiogenesis and invasiveness *via* EGFR/VEGFR-2-mediated pathwayin breast cancer. *Cell Prolif* 2016;**49**:678−97.
44. Fan JX, Zheng DW, Rong L, Zhu JY, Hong S, Li C, et al. Targeting epithelial−mesenchymal transition: metal organic network nanocomplexes for preventing tumor metastasis. *Biomaterials* 2017;**139**:116−26.
45. Thiery JP, Acloque H, Huang RYJ, Nieto MA. Epithelial−mesenchymal transitions in development and disease. *Cell* 2009;**139**:871−90.
46. Cui YN, Yang YD, Ma MC, Xu Y, Sui JH, Li HF, et al. Reductive responsive micelle overcoming multidrug resistance of breast cancer by co-delivery DOX and specific antibiotic. *J Mater Chem B* 2019;**7**:6075−86.